articles

Formulation and Characterization of Echogenic Lipid−Pluronic Nanobubbles

**Tianyi M. Krupka,†,‡ Luis Solorio,‡ Robin E. Wilson,‡ Hanping Wu,† Nami Azar,†
and Agata A. Exner*,†**

*Departments of Radiology and Biomedical Engineering, Case Western Reserve University,
Cleveland, Ohio 44106*

Abstract: The advent of microbubble contrast agents has enhanced the capabilities of ultrasound as a medical imaging modality and stimulated innovative strategies for ultrasound-mediated drug and gene delivery. While the utilization of microbubbles as carrier vehicles has shown encouraging results in cancer therapy, their applicability has been limited by a large size which typically confines them to the vasculature. To enhance their multifunctional contrast and delivery capacity, it is critical to reduce bubble size to the nanometer range without reducing echogenicity. In this work, we present a novel strategy for formulation of nanosized, echogenic lipid bubbles by incorporating the surfactant Pluronic, a triblock copolymer of ethylene oxide copropylene oxide coethylene oxide into the formulation. Five Pluronics (L31, L61, L81, L64 and P85) with a range of molecular weights (M_w: 1100 to 4600 Da) were incorporated into the lipid shell either before or after lipid film hydration and before addition of perfluorocarbon gas. Results demonstrate that Pluronic−lipid interactions lead to a significantly reduced bubble size. Among the tested formulations, bubbles made with Pluronic L61 were the smallest with a mean hydrodynamic diameter of 207.9 ± 74.7 nm compared to the 880.9 ± 127.6 nm control bubbles. Pluronic L81 also significantly reduced bubble size to 406.8 ± 21.0 nm. We conclude that Pluronic is effective in lipid bubble size control, and Pluronic M_w, hydrophilic−lipophilic balance (HLB), and Pluronic/ lipid ratio are critical determinants of the bubble size. Most importantly, our results have shown that although the bubbles are nanosized, their stability and in vitro and in vivo echogenicity are not compromised. The resulting nanobubbles may be better suited for contrast enhanced tumor imaging and subsequent therapeutic delivery.

Keywords: Ultrasound Contrast Agent; Pluronic; Nanobubbles; Lipid; Surfactant

Introduction

Ultrasound contrast agents (UCA) are small gas-filled bubbles with a stabilizing shell made from a variety of materials such as polymer,[1−4] protein[5,6] or lipid.[7−9] Other than the traditional applications of these agents in diagnostic ultrasound imaging,[10,11] UCA have found relevance in therapeutic applications including targeted gene[12−14] and

* To whom correspondence should be addressed: Agata A. Exner, Ph.D., Department of Radiology, Case Western Reserve University, 11100 Euclid Avenue, Cleveland, OH 44106-5056. E-mail: agata.exner@case.edu. Phone: (216) 844-3544. Fax: (216) 844-5922.
† Department of Radiology.
‡ Biomedical Engineering.

(1) Wheatley, M. A.; Schrope, B.; Shen, P. Contrast agents for diagnostic ultrasound: development and evaluation of polymer-coated microbubbles. *Biomaterials* **1990**, *11* (9), 713–7.

(2) Schneider, M.; et al. BR1: a new ultrasonographic contrast agent based on sulfur hexafluoride-filled microbubbles. *Invest. Radiol.* **1995**, *30* (8), 451–7.

(3) Bjerknes, K.; et al. Air-filled polymeric microcapsules from emulsions containing different organic phases. *J. Microencapsulation* **2001**, *18* (2), 159–71.

(4) Cavalieri, F.; et al. Stable polymeric microballoons as multifunctional device for biomedical uses: synthesis and characterization. *Langmuir* **2005**, *21* (19), 8758–64.

drug delivery.[14−22] These adaptable particles are currently being explored as protective therapeutic carriers[23,24] and as cavitation nuclei to enhance delivery of their payload by

sonoporation.[25] Together these functions improve payload circulation half-life and release profiles as well as tissue selectivity and cell uptake. Regardless of the mode of action, it is advantageous, particularly in cancer therapy, for the bubble size to be in the nanometer range in order for the bubbles to extravasate from the vasculature and arrive at the cellular target site for the desired effect.

Commercial UCA available today are typically designed to serve only as blood pool agents with diameters of $1-8$ μm.[26] Although previous methodologies have been developed to reduce bubble size, most of these strategies involve manipulations of microbubbles post formulation, such as gradient separation by gravitational forces or by physical filtration or floatation.[27,28] While effective for selecting nanosized bubbles, these methods introduce potential for sample contamination, reduce bubble yield and stability, and waste stock materials in addition to being labor intensive.[29] In this work we present a simple strategy using Pluronic as a size control excipient to produce nanosized lipid bubbles.

Pluronics (also known as poloxamers), or polyethylene oxide (EO$_x$)-polypropylene oxide (PO$_y$)-polyethylene oxide (EO$_x$), are a family of nonionic triblock copolymers (M_w: $1100-14600$) once classified as "inactive excipients" by the FDA. These amphiphilic surfactants are commonly used in industrial applications as antifoaming agents, cosmetics, pharmaceuticals as emulsifiers[30] and colloidal dispersion stabilizers,[31,32] supplement for cell culture media.[33−35]

(5) Feinstein, S. B.; et al. Safety and efficacy of a new transpulmonary ultrasound contrast agent: initial multicenter clinical results. *J. Am. Coll. Cardiol.* **1990**, *16* (2), 316–24.

(6) Dayton, P. A.; et al. Optical and acoustical observations of the effects of ultrasound on contrast agents. *IEEE Trans. Ultrasonics, Ferroelectr., Freq. Control* **1999**, *46* (1), 220–32.

(7) Ferrara, K. W.; Borden, M. A.; Zhang, H. Lipid-Shelled Vehicles: Engineering for Ultrasound Molecular Imaging and Drug Delivery. *Acc. Chem. Res.* **2009**, *42* (7), 881–92.

(8) Unger, E. C.; et al. Therapeutic applications of lipid-coated microbubbles. *Adv. Drug Delivery Rev.* **2004**, *56* (9), 1291–314.

(9) Zheng, H.; et al. A sensitive ultrasonic imaging method for targeted contrast microbubble detection. *Conf. Proc. IEEE Eng. Med. Biol. Soc.* **2008**, *2008*, 5290–3.

(10) Miller, A. P.; Nanda, N. C. Contrast echocardiography: new agents. *Ultrasound Med. Biol.* **2004**, *30* (4), 425–34.

(11) Tang, J.; et al. Evaluation of the effect of protamine on human prostate carcinoma PC-3m using contrast enhanced Doppler ultrasound. *J. Urol.* **2003**, *170* (2 Part 1), 611–4.

(12) Crowder, K. C.; et al. Sonic activation of molecularly-targeted nanoparticles accelerates transmembrane lipid delivery to cancer cells through contact-mediated mechanisms: implications for enhanced local drug delivery. *Ultrasound Med. Biol.* **2005**, *31* (12), 1693–700.

(13) Larina, I. V.; et al. Enhancement of drug delivery in tumors by using interaction of nanoparticles with ultrasound radiation. *Technol. Cancer Res. Treat.* **2005**, *4* (2), 217–26.

(14) Chumakova, O. V.; et al. Composition of PLGA and PEI/DNA nanoparticles improves ultrasound-mediated gene delivery in solid tumors in vivo. *Cancer Lett.* **2008**, *261* (2), 215–25.

(15) Fang, J. Y.; et al. Acoustically active perfluorocarbon nanoemulsions as drug delivery carriers for camptothecin: drug release and cytotoxicity against cancer cells. *Ultrasonics* **2009**, *49* (1), 39–46.

(16) Lindner, J. R.; et al. Microbubble persistence in the microcirculation during ischemia/reperfusion and inflammation is caused by integrin- and complement-mediated adherence to activated leukocytes. *Circulation* **2000**, *101* (6), 668–75.

(17) Kheirolomoom, A.; et al. Acoustically-active microbubbles conjugated to liposomes: characterization of a proposed drug delivery vehicle. *J. Controlled Release* **2007**, *118* (3), 275–84.

(18) Bekeredjian, R.; et al. Ultrasound-targeted microbubble destruction can repeatedly direct highly specific plasmid expression to the heart. *Circulation* **2003**, *108* (8), 1022–6.

(19) Husseini, G. A.; Pitt, W. G. Ultrasonic-activated micellar drug delivery for cancer treatment. *J. Pharm. Sci.* **2009**, *98* (3), 795–811.

(20) Rapoport, N.; Gao, Z.; Kennedy, A. Multifunctional nanoparticles for combining ultrasonic tumor imaging and targeted chemotherapy. *J. Natl. Cancer Inst.* **2007**, *99* (14), 1095–106.

(21) Husseini, G. A.; et al. Release of doxorubicin from unstabilized and stabilized micelles under the action of ultrasound. *J. Nanosci. Nanotechnol.* **2007**, *7* (3), 1028–33.

(22) Frenkel, V. Ultrasound mediated delivery of drugs and genes to solid tumors. *Adv. Drug Delivery Rev.* **2008**, *60* (10), 1193–208.

(23) Lum, A. F.; et al. Ultrasound radiation force enables targeted deposition of model drug carriers loaded on microbubbles. *J. Controlled Release* **2006**, *111* (1−2), 128–34.

(24) Bekeredjian, R.; et al. Augmentation of cardiac protein delivery using ultrasound targeted microbubble destruction. *Ultrasound Med. Biol.* **2005**, *31* (5), 687–91.

(25) Gao, Z.; Fain, H. D.; Rapoport, N. Ultrasound-enhanced tumor targeting of polymeric micellar drug carriers. *Mol. Pharmaceutics* **2004**, *1* (4), 317–30.

(26) Ferrara, K. W.; Borden, M. A.; Zhang, H. Lipid-shelled vehicles: engineering for ultrasound molecular imaging and drug delivery. *Acc. Chem. Res.* **2009**, *42* (7), 881–92.

(27) Goertz, D. E.; et al. High-frequency, nonlinear flow imaging of microbubble contrast agents. *IEEE Trans. Ultrasonics, Ferroelectr., Freq. Control* **2005**, *52* (3), 495–502.

(28) Zong, Y.; et al. Optimal design and experimental investigation of surfactant encapsulated microbubbles. *Ultrasonics* **2006**, *44* (Suppl. 1), e119−22.

(29) Hwang, T. L.; et al. Development and evaluation of perfluorocarbon nanobubbles for apomorphine delivery. *J. Pharm. Sci.* **2009**, *98* (10), 3735–47.

(30) Ivanova, R.; Lindman, B.; Alexandridis, P. Effect of pharmaceutically acceptable glycols on the stability of the liquid crystalline gels formed by Poloxamer 407 in water. *J. Colloid Interface Sci.* **2002**, *252* (1), 226–35.

(31) Sakai, T.; Alexandridis, P. Single-step synthesis and stabilization of metal nanoparticles in aqueous pluronic block copolymer solutions at ambient temperature. *Langmuir* **2004**, *20* (20), 8426–30.

(32) Sakai, T.; Alexandridis, P. Spontaneous formation of gold nanoparticles in poly(ethylene oxide)-poly(propylene oxide) solutions: solvent quality and polymer structure effects. *Langmuir* **2005**, *21* (17), 8019–25.

(33) Tharmalingam, T.; et al. Pluronic enhances the robustness and reduces the cell attachment of mammalian cells. *Mol. Biotechnol.* **2008**, *39* (2), 167–77.

(34) Michaels, J. D.; et al. Interfacial properties of cell culture media with cell-protecting additives. *Biotechnol. Bioeng.* **1995**, *47* (4), 420–30.

Because of their relatively nontoxic nature, the applications of Pluronics in experimental medicine and pharmaceutical sciences can be traced far back.[36,37] In recent years, functional applications of Pluronic as a chemo[38−46] and thermal sensitizing agent[47,48] to cancer treatment have also been explored and shown to hold some promise in modifying biological cancer cell response. The goal of this work was to investigate the Pluronic effects in formulation of perfluorocarbon lipid-shelled bubbles for use as ultrasound contrast agents and, eventually, delivery vehicles for cancer diagnosis and therapy.

Materials and Methods

Pluronic P85 and L61 were donated by BASF (Shreveport, LA). Other Pluronic products (Table 1) and glycerol were purchased from Sigma Aldrich (Milwaukee, WI). Octaflouropropane (C_3F_8) gas was purchased from American Gas Group (Toledo, OH). Dulbecco's phosphate buffered saline

Table 1. Pluronic Information

pluronic	formula	M_w (Da)	HLB	PO/EO ratio	CMC (M; wt %)
L31	EO_2-PO_{16}-EO_2	1100	1−7	8	N/A
L61	EO_2-PO_{31}-EO_2	2000	1−7	13.6	$1.1 \times 10-4$; 0.022
L81	EO_3-PO_{43}-EO_3	2750	1−7	13.7	$2.3 \times 10-5$; 0.0063
L64	EO_{13}-PO_{30}-EO_{13}	2900	12−18	2.3	$4.8 \times 10-4$; 0.14
P85	EO_{26}-PO_{40}-EO_{26}	4600	16	1.5	$6.5 \times 10-5$; 0.03

Table 2. Experimental Information

[Pluronic] (mg/mL)	0.006	0.06	0.6	6
Pluronic mass %	0.075	0.75	7.5	75
Lipid/Pluronic Molar Ratio				
L31	2051.9	205.2	20.5	
L61	3730.8	373.1	37.3	
L81	5409.7	541.0	54.1	
L64	5129.9	513.0	51.3	
P85		858.1	85.8	8.6

(PBS) was purchased from GIBCO (Grand Island, NY). Lipids, 1,2-dipalmitoyl-*sn*-glycero-3-phosphocholine (DPPC; M_w: 734.05), 1,2-dipalmitoyl-*sn*-glycero-3-phosphoethanolamine (DPPE; M_w: 691.97), and 1,2-dipalmitoyl-*sn*-glycero-3-phosphate (DPPA; M_w: 670.88) in powder form were purchased from Avanti Polar Lipids Inc. (Pelham, AL) and used without further purification.

Bubble Formation. Bubbles were prepared by first dissolving DPPC, DPPA and DPPE in chloroform, followed by evaporation of the solvent and hydration with $1\times$ PBS in the presence of glycerol to produce lipid vesicles. To formulate Pluronic bubbles, Pluronic (Table 2) was either codissolved in the chloroform lipid solution before solvent evaporation (prefilm) or was added to the hydration PBS/glycerol solution (postfilm). Hydration of the lipid films took place at 37 °C in an incubator-shaker at 120 rpm for 60 min (New Brunswick Scientific). Next, the vials were sealed, the air was withdrawn by a syringe and octafluoropropane was added to the vials until the pressure in the vial was equalized. Finally, the vial was placed on a VialMix shaker (Bristol-Myers Squibb Medical Imaging, Inc., N. Billerica, MA) for 45 s to form the bubbles. Samples were placed on ice immediately after formulation and stored for analysis.

Bubble Sizing and Stability. Bubble size was measured by dynamic light scattering using photon correlation spectroscopy (PCS) at 25 °C (90Plus Brookhaven Instruments Corp). The analysis was done with a laser wavelength of 660 nm at an angle of 90°. Bubble stability in solution over 1 h was analyzed with dynamic light scattering to examine the potential of the bubbles to coalesce. Briefly, 10 μL of bubble stock solution was dissolved in 3 mL of 1 mM KCl in a cuvette at room temperature. Bubble size was determined as above at 0, 15, 30, 45, 60 min. The shift in size distribution and polydispersity was noted. These experiments were repeated in triplicate. All bubble sizes presented are based on the number average calculations.

(35) Michaels, J. D.; et al. Analysis of cell-to-bubble attachment in sparged bioreactors in the presence of cell-protecting additives. *Biotechnol. Bioeng.* **1995**, *47* (4), 407–19.

(36) Schmolka, I. R. Theory of emulsions. *Fed. Proc.* **1970**, *29* (5), 1717–20.

(37) Schmolka, I. R. Artificial blood emulsifiers. *Fed. Proc.* **1975**, *34* (6), 1449–53.

(38) Spitzenberger, T. J.; et al. Novel delivery system enhances efficacy of antiretroviral therapy in animal model for HIV-1 encephalitis. *J. Cereb. Blood Flow Metab.* **2007**, *27* (5), 1033–42.

(39) Alakhov, V.; et al. Hypersensitization of multidrug resistant human ovarian carcinoma cells by pluronic P85 block copolymer. *Bioconjugate Chem.* **1996**, *7* (2), 209–16.

(40) Batrakova, E. V.; et al. Effects of pluronic P85 unimers and micelles on drug permeability in polarized BBMEC and Caco-2 cells. *Pharm. Res.* **1998**, *15* (10), 1525–32.

(41) Batrakova, E. V.; et al. Sensitization of cells overexpressing multidrug-resistant proteins by pluronic P85. *Pharm. Res.* **2003**, *20* (10), 1581–90.

(42) Kabanov, A. V.; Batrakova, E. V.; Miller, D. W. Pluronic block copolymers as modulators of drug efflux transporter activity in the blood-brain barrier. *Adv. Drug Delivery Rev.* **2003**, *55* (1), 151–64.

(43) Krupka, T. M.; et al. Effect of intratumoral injection of carboplatin combined with pluronic P85 or L61 on experimental colorectal carcinoma in rats. *Exp. Biol. Med. (Maywood)* **2007**, *232* (7), 950–7.

(44) Krupka, T. M.; et al. Injectable polymer depot combined with radiofrequency ablation for treatment of experimental carcinoma in rat. *Invest. Radiol.* **2006**, *41* (12), 890–7.

(45) Minko, T.; et al. Pluronic block copolymers alter apoptotic signal transduction of doxorubicin in drug-resistant cancer cells. *J. Controlled Release* **2005**, *105* (3), 269–78.

(46) Venne, A.; et al. Hypersensitizing effect of pluronic L61 on cytotoxic activity, transport, and subcellular distribution of doxorubicin in multiple drug-resistant cells. *Cancer Res.* **1996**, *56* (16), 3626–9.

(47) Weinberg, B. D.; et al. Combination of sensitizing pretreatment and radiofrequency tumor ablation: evaluation in rat model. *Radiology* **2008**, *246* (3), 796–803.

(48) Krupka, T. M.; Dremann, D.; Exner, A. A. Time and dose dependence of pluronic bioactivity in hyperthermia-induced tumor cell death. *Exp. Biol. Med. (Maywood)* **2009**, *234* (1), 95–104.

Concurrently, bubbles were exposed to $1\times$ PBS that was preheated to 37 °C in a water bath for 0 to 60 min. At predetermined time points, bubble samples were transferred to a hemacytometer and three images ($400\times$) at random fields at each time point per sample were acquired (microscope: Zeiss Axioskop, WEL Instrument CO. LLC; Camera: Zeiss Axiocam MRc5). The number of visible bubbles per image was counted by a custom Matlab program. This program isolated the center of the bubbles and excluded objects based on the size and eccentricity of the object counted. These experiments were also carried out in triplicate. It is important to note that because the smaller-sized bubbles were beyond the resolution of our imaging system; this experiment provides information on stability of the relatively larger bubble (0.4−8 μm) populations.

Zeta Potential Measurements. Zeta potential of each sample was measured using a Zeta Plus Analyzer (Brookhaven Instruments Corp.) by Laser Doppler Anemometry (LDA) using electrophoretic light scattering at 25 °C. Test samples for these studies were prepared identically as those for DLS sizing measurements. Dilute particle concentration was maintained to ensure that multiple scattering and particle−particle interactions were negligible. Each sample was run using five repetitions, and the average was taken as the final zeta potential.

Bubble Echogenicity in Vitro. In order to characterize the inherent bubble echogenicity with minimal external disturbance, grayscale intensity changes generated by the bubbles were measured in vitro using a linear transducer (Toshiba, Tochigi-Ken, Japan) and a clinical ultrasound scanner (Toshiba Aplio) at 14 MHz (gain, 88; mechanical index, <0.1; see Figure 4A,B for experimental setup). To carry out the measurements, 400 μL of bubble solution either at the same dilution of stock solution (1:1000) or at the same concentration (3.6×10^5 bubbles/mL) approximated from the initial hemacytometer data were injected into a custom-designed agarose mold (1% agarose, 99% H_2O). Five images of each sample were acquired. The grayscale image intensity was measured with a custom Matlab program, which calculated the mean grayscale value of all nonzero elements in a selected region of interest. This data was normalized to the control. Furthermore, in order to approximate the signal generated by each bubble in the samples of equal dilution (since the absolute number of nanobubbles was considerably greater than that of microbubbles) the signal intensity of each bubble was determined based on the hemacytometer counts and normalized to that of control bubbles.

In addition, since the light microscopy technique has a limited spatial resolution (typically visualizing bubbles >200 nm in diameter), the change in grayscale signal intensity of bubble solution over time was examined to gain further insight regarding stability of the overall bubble population. Samples were diluted (1:1000) in PBS. At $t = 0$, 10, 20, and 30 min, 400 μL of sample was transferred to the agarose mold and, as above, five images of each bubble sample were acquired. Here, the grayscale signal intensity of a manually selected region of interest was measured using ImageJ.

Measurements at each time point were normalized to the initial values of each sample.

In Vivo Assessment of Nanobubble Contrast. All animals were housed in accordance with the Guide for the Care and Use of Laboratory Animals adopted by the National Institutes of Health; and all animal procedures were approved by the Institutional Animal Care and Use Committee at Case Western Reserve University. Ten week old female rats (Charles River, Wilmington, MA) carrying subcutaneous tumors with size range of 13.16−15.87 mm were used in this study. The tumors were inoculated by injection of 1.0 $\times 10^5$ DHD/K12/TRb rat colorectal adenocarcinoma cells originating from chemically induced adenocarcinoma in the same strain.[43] From the in vitro characterization studies above, the smallest bubbles (those made with Pluronic L61) were selected for the following experiments. To examine nanobubble contrast dynamics in vivo, Pluronic L61 nanobubbles (hydrostatic diameter range: 103−279 nm) and control microbubbles (hydrostatic diameter range: 0.94−1.03 μm) were administered to tumor bearing rats (anesthetized with isoflurane) via bolus injection of 50 μL of bubbles followed by 0.8 mL flush with normal saline into the tail vein. To acquire images, the US probe was immobilized using a clamp and a gel pad was placed between the probe and tumor. After the identification of the tumor with 2D Doppler, harmonic perfusion imaging was used to image changes in the tissue contrast density with time. Images were acquired with a 6 MHz linear transducer (PLT604AT; gain, 90; mechanical index, 0.1). Initial image acquisition was started 10 s before bubble administration and completed after 60 s. Subsequently, 10 s video clips were acquired at $t = 5$, 10, 15, and 20 min. Each tumor (8 tumors in 8 animals) received both control bubbles and Pluronic nanobubbles separately in a random order 40 min apart.

Image analysis was performed by registering the image series at each time point to the $t = 0$ images using 2D rigid body registration. The transformation optimization was performed with Matlab, using the Nelder−Mead simplex algorithm function based on gray scale similarity, to minimize the sum of the squared difference between prebubble injection and postinjection images. Goodness of fit was evaluated by comparing the distance between image edges using a mosaic overlay. The region of interest was then selected, and the mean gray scale value of the ROI was calculated. After the mean gray scale value was calculated for all time points, the images were normalized by the preinjection (baseline) value for each animal and the normalized baseline value was subtracted from each time point to give the fold enhancement. To ensure proper registration, the $t = 0$ images were registered to themselves.

To further examine contrast dynamics, an additional study was performed using contrast enhanced microflow imaging (MFI). By combining a flash-replenishment (FR) sequence and max-hold processing,[49] MFI has been demonstrated as

(49) Kamiyama, N. Update of ultrasound contrast imaging. *Int. Congr. Ser.* **2004**, *1274*, 53–56.
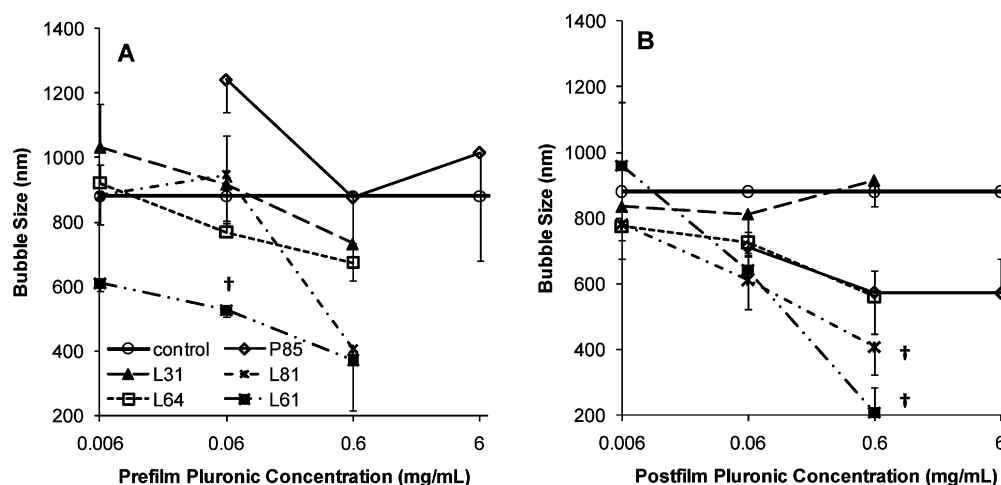
Figure 1. Bubble size in the presence of 0.006, 0.06, 0.6, and 6 mg/mL of Pluronic that was incorporated into the bubble formulation before (A: prefilm) or after (B: postfilm) lipid film hydration (mean $\pm$ SEM; $n = 3$). The symbol † indicates statistically significant difference compared to control (P: 0.001−0.01).

an excellent tool for revealing the vascular network of lesions.[50,51] In this imaging procedure, the FR sequence destroys all bubbles in the imaging plane using a burst scan at high MI (set by the manufacturer). Subsequently, during the bubble replenish phase, the maximum bubble intensity at each location is collected and stored until a higher intensity signal at the same location is reached. Then, this higher signal intensity is registered and replaces the previous value using max-hold processing. In this study, using MFI, movies were acquired immediately after bubble injection for 30 s (MI, 0.1; frame rate, 15 frames/s; auto replenish rate, every 10 s; dynamic range, 90 dB; acoustic frame rate, 45 frames/s). The max-hold processing was realized at low mechanical index (MI: 0.1). MFI data were recorded as AVI clips, and ImageJ was used to extract each video frame. From each video, the first complete 10 s of the time intensity (TI) data were extracted and compared.

Statistical Analysis. Two-tailed, unpaired Student's t test was performed for comparisons of all treatment groups. For multiple comparisons, significance levels were corrected using a Bonferroni adjustment. Unless otherwise noted, all data is reported as mean $\pm$ SEM (standard error of mean). A P value ≤ 0.05 was considered statistically significant before Bonferroni correction.

Results

Bubble Size. Five Pluronics at four different concentrations were tested for their ability to control lipid bubble size (Figure 1). All Pluronic bubbles were relatively monodispersed with a polydispersity index ranging from 0.005 to 0.296 (Table 3), and all but one (prefilm 0.06 mg/mL P85) had smaller or comparable sizes relative to control bubbles.

(50) Linden, R. A.; et al. Contrast enhanced ultrasound flash replenishment method for directed prostate biopsies. *J. Urol.* **2007**, *178* (6), 2354–8.

(51) Hotta, N.; et al. Advanced dynamic flow imaging with contrast-enhanced ultrasonography for the evaluation of tumor vascularity in liver tumors. *Clin. Imaging* **2005**, *29* (1), 34–41.

Smallest bubbles were those made with Pluronic L61 (0.6 mg/mL postfilm 207.9 ± 74.7 nm, $P = 0.001$ compared to control bubbles; and prefilm 371.6 ± 156.3 nm, $P = 0.05$ compared to control bubbles;) followed by L81 (0.6 mg/mL postfilm 407.2 ± 84.3 nm, $P = 0.01$ compared to control bubbles; and prefilm 406.8 ± 21.0 nm, $P = 0.006$ compared to control bubbles). P85 bubbles were larger than control bubbles with prefilm P85 bubbles significantly larger than control bubbles (0.06 mg/mL prefilm: 1241.0 ± 99.6 nm; $P = 0.05$).

Bubble Size Distribution Change as a Function of Time. Bubble size was monitored up to 60 min to examine the tendency of the bubbles to coalesce and form larger bubbles. With the exception of P85 bubbles, bubble size remained relatively constant and showed no significant increase within the 60 min analysis period (Figure 2). For clarity, data is shown only for bubbles with 0.6 mg/mL Pluronic. Bubbles made with the postfilm addition of Pluronic appeared to show less size variation over the time period, and bubbles with L61 and L81 showed the most consistent stability. All bubbles in the presence of P85 showed a time dependent size growth.

Bubble Rate of Dissolution. The relative change in bubble stability was monitored for 60 min at 37 °C in vitro. Here, stability was defined as the robustness or rate of dissolution of bubbles in solution. Data were normalized based on the initial bubble concentrations at $t = 0$. Again, for clarity, representative data of control bubbles and bubbles at 0.6 mg/mL of Pluronic are presented (Figure 3). In general postfilm bubbles appeared to have better stability compared to prefilm bubbles, but in both groups, bubble loss was evident after 15 min. All bubble concentrations (P: 0.0001−0.023) decreased significantly at $t = 60$ min compared to that at $t = 0$, except prefilm L31 bubbles ($P = 0.1$). After 60 min, control bubbles decreased to $60.8 \pm 8.4\%$ ($P < 0.001$) of their initial concentration compared to 19.2 to 74.8% for prefilm Pluronic bubbles, and 20.4 to 84.4% for postfilm Pluronic bubbles. Again, it is important to note that because

Table 3. Summary of Lipid−Pluronic Bubble Characterization

	[Pluronic] (mg/mL)	diameter[a] (nm) (prefilm; postfilm)	polydispersity (prefilm; postfilm)	zeta (mV) (prefilm; postfilm)
control	0	880.9 ± 127.6	0.099 ± 0.032	-55.6 ± 4.2
L31	0.006	$1033.2 \pm 133.7; 835.7 \pm 75.1$	$0.005 \pm 0; 0.005 \pm 0$	$-46.0 \pm 6.5;\ -48.5 \pm 5.1$
	0.06	$917.9 \pm 149.4; 812.3 \pm 125.1$	$0.005 \pm 0; 0.104 \pm 0.055$	$-55.6 \pm 6.5;\ -54.1 \pm 11.8$
	0.6	$733.5 \pm 159.4; 915.3 \pm 77.4$	$0.296 \pm 0.010; 0.133 \pm 0.036$	$-54.4 \pm 1.2;\ -52.0 \pm 6.2$
L61	0.006	$609.8 \pm 24.2; 959.3 \pm 194.4$	$0.005 \pm 0; 0.107 \pm 0.084$	$-5.8 \pm 12.5;\ -50.3 \pm 1.1$
	0.06	$526.4 \pm 20.9;^\dagger 641.8 \pm 53.0$	$0.124 \pm 0.075; 0.162 \pm 0.058$	$-64.0 \pm 5.7;\ -47.6 \pm 3.1$
	0.6	$371.6 \pm 156.3; 207.9 \pm 74.7^\dagger$	$0.225 \pm 0.044; 0.227 \pm 0.055$	$-64.7 \pm 4.4;\ -44.3 \pm 2.7$
L81	0.006	$882.1 \pm 90.0; 782.1 \pm 47.9$	$0.005 \pm 0; 0.053 \pm 0.048$	$-41.6 \pm 2.6;\ -40.9 \pm 4.5$
	0.06	$946.8 \pm 151.8; 611.3 \pm 90.0$	$0.207 \pm 0.054; 0.236 \pm 0.032$	$-37.4 \pm 3.4;\ -42.3 \pm 1.1$
	0.6	$406.8 \pm 21.0;^\dagger 407.2 \pm 84.3^\dagger$	$0.144 \pm 0.073; 0.117 \pm 0.073$	$-39.4 \pm 1.0;\ -40.3 \pm 2.0$
L64	0.006	$920.8 \pm 58.2; 774.5 \pm 100.2$	$0.005 \pm 0; 0.005 \pm 0$	$-41.6 \pm 2.6;\ -56.6 \pm 2.6$
	0.06	$769.0 \pm 36.3; 726.3 \pm 42.6$	$0.093 \pm 0.047; 0.082 \pm 0.077$	$-46.9 \pm 0.9;\ -44.4 \pm 1.6$
	0.6	$674.6 \pm 61.2; 561.0 \pm 111.9$	$0.224 \pm 0.019; 0.242 \pm 0.025$	$-39.9 \pm 6.3;\ -36.7 \pm 5.9$
P85	0.06	$1241.0 \pm 99.6;^\ddagger 711.8 \pm 45.1$	$0.095 \pm 0.048; 0.138 \pm 0.055$	$-54.9 \pm 10.0;\ -49.4 \pm 1.7$
	0.6	$874.6 \pm 256.8; 573.2 \pm 67.6$	$0.292 \pm 0.042; 0.206 \pm 0.061$	$-66.4 \pm 6.2;\ -53.3 \pm 7.6$
	6	$1015 \pm 335.3; 570.9 \pm 105.8$	$0.200 \pm 0.039; 0.295 \pm 0.016$	$-60.6 \pm 7.7;\ -45.8 \pm 6.0$

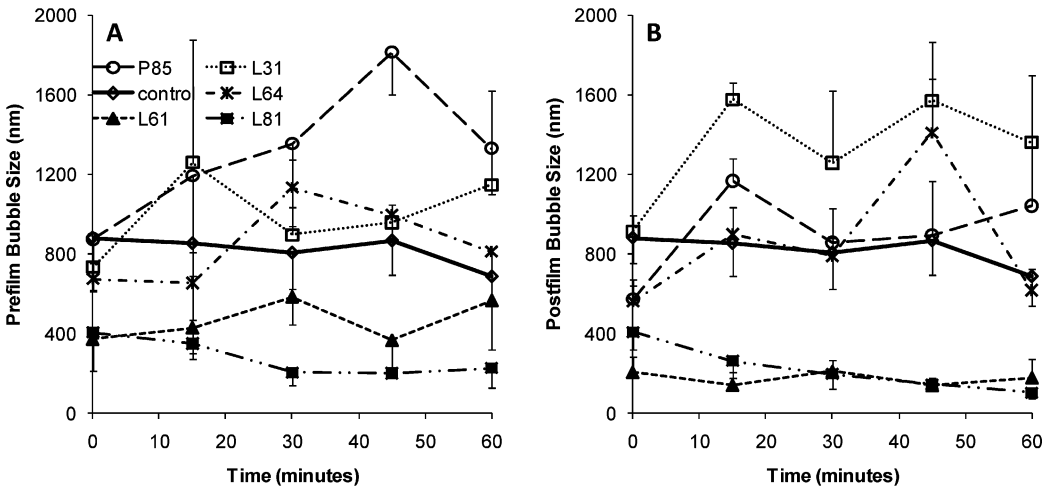[a] (†) Significant difference vs control; (‡) significant difference vs postfilm.

Figure 2. Bubble size distribution change as a function of time. Data presented for control bubbles and bubbles with 0.6 mg/mL of Pluronic (mean ± SEM; $n = 3$). (A) Prefilm; (B) postfilm.
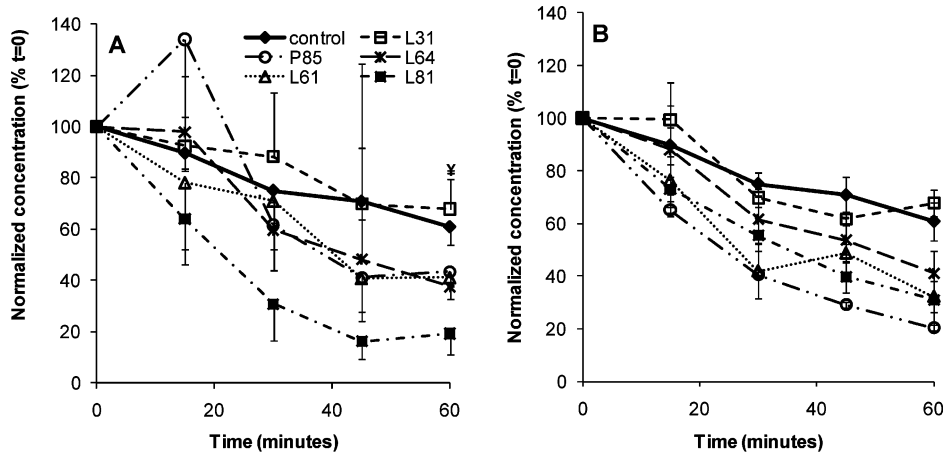

Figure 3. Bubble concentration change as a function of time (A, prefilm; B, postfilm; P: 0.0001−0.023). Data presented as mean ± SEM ($n = 3$). The symbol ¥ indicates the only condition that showed no significant difference at $t = 60$ min vs $t = 0$ ($P = 0.1$).

these stability measurements were carried out using microscopy, it is possible that smaller bubbles were omitted in the final analysis. This may account for the apparently lower stability of the nanosized vehicles.
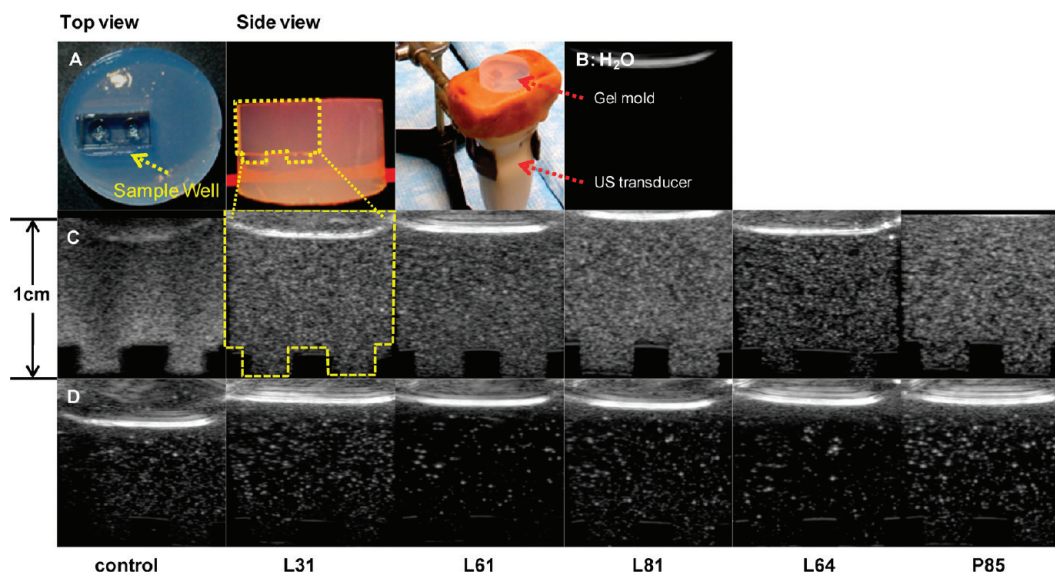
Figure 4. Representative control, Pluronic bubble grayscale ultrasound images in vitro in custom-made agarose gel mold and experimental setup (A); dashed line indicates sample well; (B) US image of H_2O; (C) bubbles with 0.6 mg/mL of L31, L61, L81, L64 and P85 at same dilutions; (D) control, bubbles with 0.6 mg/mL of L31, L61, L81, L64 and P85 at equivalent bubble concentrations.

Zeta Potential. Zeta potential measurement provides information on the stability of particle in suspension and is a function of particle surface charge[52] (Table 3). Our results showed that control bubbles had net negative charge of −55.6 ± 4.2 mV. These bubbles are stable and have a negatively charged surface due to the presence of DPPA. In the presence of Pluronic, no significant difference in bubble surface charge was detected; the zeta potentials ranged between −64.7 ± 4.4 mV and −37.4 ± 3.4 mV for prefilm Pluronic, and between −50.3 ± 1.1 mV and −40.3 ± 2.0 mV for postfilm Pluronic bubbles.

Bubble Ultrasound Signal Intensity. The grayscale ultrasound signal intensity was quantified to determine the change in signal for each bubble formulation. Ultrasound images were acquired in custom-designed agarose molds (Figure 4A,B). Images of bubbles at 0.6 mg/mL of Pluronic under the same dilution (1:1000; Figure 4C) are shown. For comparison of echogenicity per bubble, Figure 4D shows images of bubbles that were diluted to the same concentration (3.6×10^5 bubbles/mL) using the initial hemacytometer counts reported above. Results confirmed that all Pluronic bubbles yield ultrasound signals comparable to larger control bubbles (Figure 5). None of the Pluronic bubbles showed significantly lower ultrasound signal intensity compared to control bubbles. In addition, bubbles with both low (prefilm, 345.3 ± 28.0%; postfilm, 53.5 ± 12.3%) and high concentrations of postfilm P85 had significantly higher grayscale signal intensity than control bubbles ($P < 0.008$). The signal intensity is reported as standardized values in accordance to previous published work.[53,54]

Grayscale Signal Intensity Changes Over Time. Figure 4A shows the experimental setup of the study (dashed lines indicate the sample well). A representative image of the sample medium, H_2O, is shown in Figure 4B. Results showed that the initial grayscale signal intensity of control microbubbles was 79.1 ± 3.0 and that of L61 nanobubbles was 74.8 ± 16.3 (mean ± SEM; $n = 3$). Most importantly, at 30 min, the signal intensity of control microbubbles decreased significantly (53.3 ± 4.7%) compared to $t = 0$ ($P = 0.0006$) while no significant decrease in the signal intensity of L61 nanobubbles was observed (70.3 ± 9.4%; Figure 6).

Nanobubble-Enhanced in Vivo Tumor Perfusion Imaging. All tested bubbles were visible in vivo (Figure 7). Data from 2/8 animals were excluded from the final analysis because of excessive signal noise. Initial tumor enhancement with L61 nanobubbles showed a 50% increase over control bubbles ($n = 6$). Five minutes post injection, the enhancement with nanobubbles was 30% less than control. At subsequent time points (10, 15, and 20 min), the enhancement was consistently greater with the nanobubbles compared to microbubbles, however the differences were not statistically significant.

(52) Kirby, B. J.; Hasselbrink, E. F., Jr. Zeta potential of microfluidic substrates: 1. Theory, experimental techniques, and effects on separations. *Electrophoresis* **2004**, *25* (2), 187–202.

(53) Korpanty, G.; et al. Monitoring response to anticancer therapy by targeting microbubbles to tumor vasculature. *Clin. Cancer Res.* **2007**, *13* (1), 323–30.

(54) Heckemann, R. A.; et al. Liver lesions: intermittent second-harmonic gray-scale US can increase conspicuity with microbubble contrast material-early experience. *Radiology* **2000**, *216* (2), 592–6.
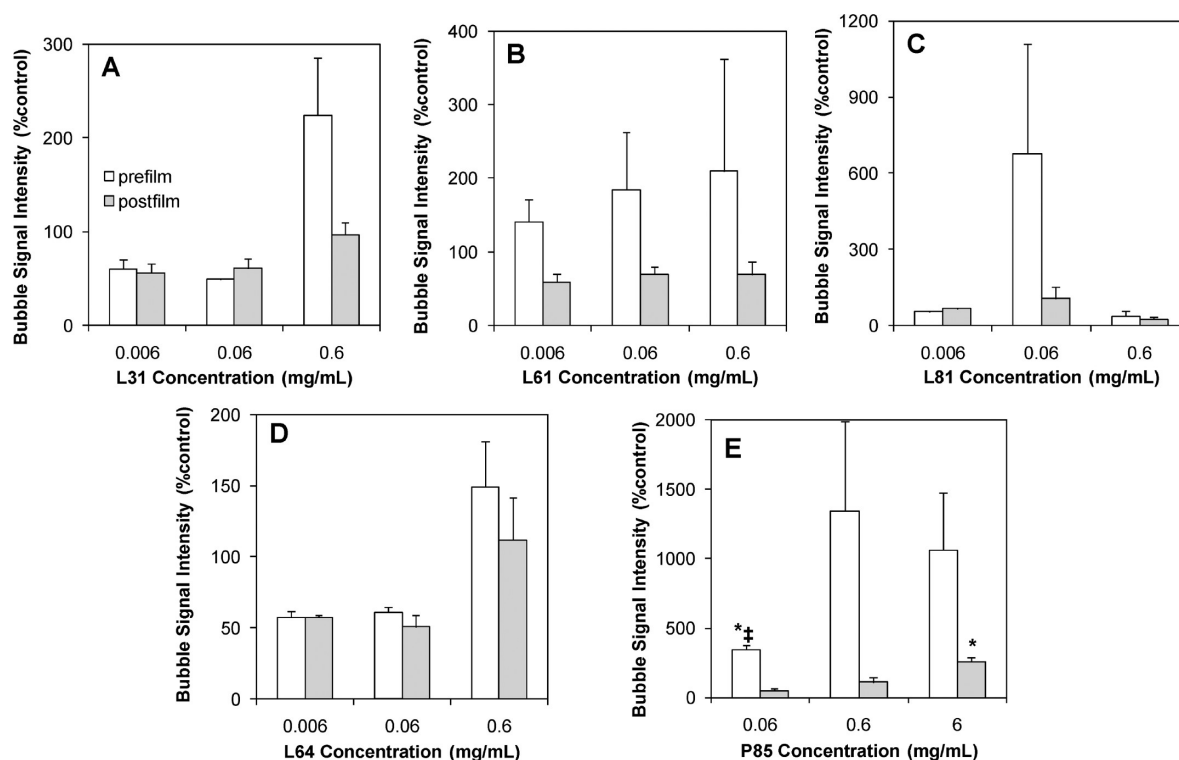
Figure 5. Quantitative analysis of grayscale ultrasound signal intensity of bubbles in the presence of 0.006, 0.06, 0.6, and 6 mg/mL of Pluronic that were incorporated in the formulation before or after lipid film hydration (mean ± SEM; n = 3). The symbol * indicates statistically significantly higher compared to control (P: 0.0006−0.008); and ‡ indicates statistically significant differences compared to postfilm bubble signals under the same conditions ($P = 0.003$). (A) L31; (B) L61; (C) L81; (D) L64; (E) P85.
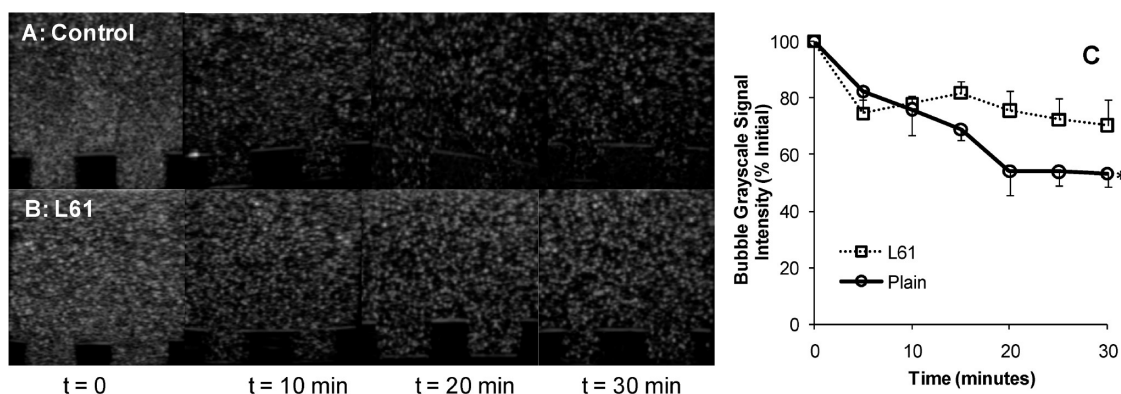
Figure 6. In vitro bubble stability. (A) Representative ultrasound images of control microbubbles and (B) L61 nanobubbles over 30 min; (C) quantatitative grayscale ultrasound signal intensity (% of initial value). The initial values of the bubble grayscale signal intensities were 79.1 ± 3.0 for control and 74.8 ± 16.3 for L61 bubbles (mean ± SEM; n = 3). The symbol * indicates statistically significant difference compared to initial value ($P = 0.0006$).

Nanobubble-Enhanced in Vivo Tumor Microflow Imaging. MFI was carried out on eight rats. One animal died immediately after control bubble injection and was excluded from the study. Figure 8A shows a representative set of MFI images of a tumor following injection of L61 nanobubbles (Figure 8B) and control microbubbles (Figure 8C). Overall 6/7 tumors showed considerably improved enhancement when imaged with L61 nanobubbles compared to control microbubbles. Contrast enhancement with nanobubbles also reached maximum intensity faster than control microbubbles.

Discussion

The goal of this work was to demonstrate the use of Pluronic triblock copolymers in simple formulation of lipid-shelled perfluorocarbon nanobubbles. Previous studies have suggested that Pluronic can stabilize nanoparticles,[31] controlling their size,[55,56] interacting with lipid membranes,[57−60] changing lipid fluidity or bubble shell elastic modulus, and

(55) Lai, J. I.; et al. Controlling the size of magnetic nanoparticles using pluronic block copolymer surfactants. *J. Phys. Chem. B* **2005**, *109* (1), 15–8.
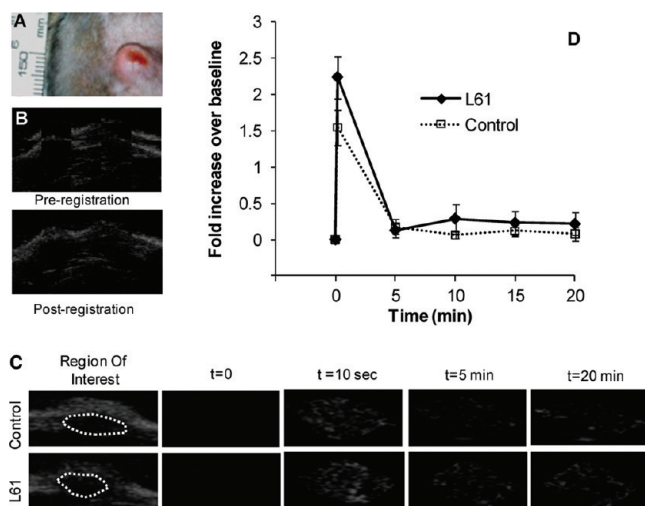
Figure 7. Bubble performance in vivo in rat tumor (perfusion imaging). (A) Representative subcutaneous tumor; (B) an example of the mosaic image used to determine quality of fit for the registration; (C) ultrasound images at $t = 0$, 10 s, 5 and 20 min after injection of control or L61 bubbles; dotted lines outline the tumors; (D) quantitative summary of tumor enhancement after contrast administration presented as fold of increase in signal intensity relative to baseline images.

preventing phagocytosis of particles by the reticuloendothelial system. A change in fluidity can control the resonant response of bubbles to ultrasound irradiation hence increase bubble echogenicity.[28,61] Here, five Pluronics with a range of M_w and hydrophobicity were examined in the formation of UCA. Results demonstrate that while all tested Pluronics play a role in modulation of bubble size, Pluronics L61 and L81 at a loading of 0.6 mg/mL were most effective in reducing it. L61 and L81 bubbles were closer to a desirable 100—300 nm range. Compared to the larger control bubbles, these nanobubbles may be more advantageous for cancer targeting in two ways. First, the small size and hydrophilic PEO segments of Pluronic, which helps transform the bubbles into

a structure similar to the stealth liposome, will likely prolong their blood pool circulation time since the larger bubbles (>1 μm) are more prone to clearance by the reticuloendothelial system (RES) after intravenous injection.[62] Second, also attributable to the small size, these nanobubbles are more likely to reach the smallest capillaries (as shown in the MFI images, Figure 8) and may be able to extravasate the leaky vasculature of tumor with more ease than the micrometer control bubbles. These properties are likely to make nanobubbles superior candidates for drug delivery or for applications in contrast enhanced tumor imagining that could take advantage of the enhanced permeability and retention effect (EPR).[63] Unlike L61 and L81, the relatively high M_w Pluronic P85 at 0.06 mg/mL resulted in bubbles that were significantly larger than control ones. The distinctive behavior between P85 and L61 or L81 may be explained by two intrinsic properties of the Pluronic molecules: the M_w[64] and hydrophilic—lipophilic balance (HLB) or relative hydrobicity. At lower Pluronic concentrations, there is a higher lipid to Pluronic molar ratio (Table 2), and the presence of Pluronic is relatively insignificant to the overall free energy of the system, thus Pluronic has minor effects on bubble size control, providing that the Pluronic has a relatively low M_w, as is the case for Pluronic L61 and L81. Unlike L61 and L81 which fit between the lipid molecules in a manner similar to cholesterol and improve the packing of the lipids in the bubbles,[65] P85 is larger, bulkier and more hydrophilic; although it is able to incorporate between the lipid molecules,[66] the long hydrophilic ethylene oxide groups protrude outside of the lipid shell increasing the overall size of the bubbles. At higher concentrations, there is a much lower lipid to Pluronic molar ratio (Table 2), and the free energy of the bubble system is disturbed by the presence of Pluronic molecules.[67] At a threshold molar ratio, some transformation becomes necessary to increase the entropy of the system to accommodate the free energy change. P85, a bulky and hydrophilic molecule, has a weaker membrane penetration ability, and the necessary transformation the system has to undergo is squeezing out P85 molecules of the lipid shell to increase the entropy.[60] Hence, at higher concentrations, P85

(56) Niesz, K.; Grass, M.; Somorjai, G. A. Precise control of the Pt nanoparticle size by seeded growth using EO13PO30EO13 triblock copolymers as protective agents. *Nano Lett.* **2005**, *5* (11), 2238–40.

(57) Frey, S. L.; Lee, K. Y. Temperature dependence of poloxamer insertion into and squeeze-out from lipid monolayers. *Langmuir* **2007**, *23* (5), 2631–7.

(58) Wu, G.; Lee, K. Y. Effects of poloxamer 188 on phospholipid monolayer morphology: an atomic force microscopy study. *Langmuir* **2009**, *25* (4), 2133–9.

(59) Frey, S. L.; et al. Effects of block copolymer's architecture on its association with lipid membranes: experiments and simulations. *J. Chem. Phys.* **2007**, *127* (11), 114904.

(60) Chang, L. C.; et al. Interactions of Pluronics with phospholipid monolayers at the air-water interface. *J. Colloid Interface Sci.* **2005**, *285* (2), 640–52.

(61) Chen, Y. C.; et al. Pluronic block copolymers: novel functions in ultrasound-mediated gene transfer and against cell damage. *Ultrasound Med. Biol.* **2006**, *32* (1), 131–7.

(62) Moghimi, S. M.; Hunter, A. C.; Murray, J. C. Long-circulating and target-specific nanoparticles: theory to practice. *Pharmacol. Rev.* **2001**, *53* (2), 283–318.

(63) Decuzzi, P.; et al. Intravascular delivery of particulate systems: does geometry really matter? *Pharm. Res.* **2009**, *26* (1), 235–43.

(64) Batrakova, E. V.; et al. Mechanism of pluronic effect on P-glycoprotein efflux system in blood-brain barrier: contributions of energy depletion and membrane fluidization. *J. Pharmacol. Exp. Ther.* **2001**, *299* (2), 483–93.

(65) Zhirnov, A. E.; et al. Lipid composition determines interaction of liposome membranes with Pluronic L61. *Biochim. Biophys. Acta* **2005**, *1720* (1–2), 73–83.

(66) Batrakova, E. V.; et al. Optimal structure requirements for pluronic block copolymers in modifying P-glycoprotein drug efflux transporter activity in bovine brain microvessel endothelial cells. *J. Pharmacol. Exp. Ther.* **2003**, *304* (2), 845–54.

(67) Inoue, T. *Vesicles*, 1st ed.; Surfactant science series; Rosoff, M., Ed.; Marcel Dekker, Inc.: New York, NY, 1996; Vol. 62, p 752.
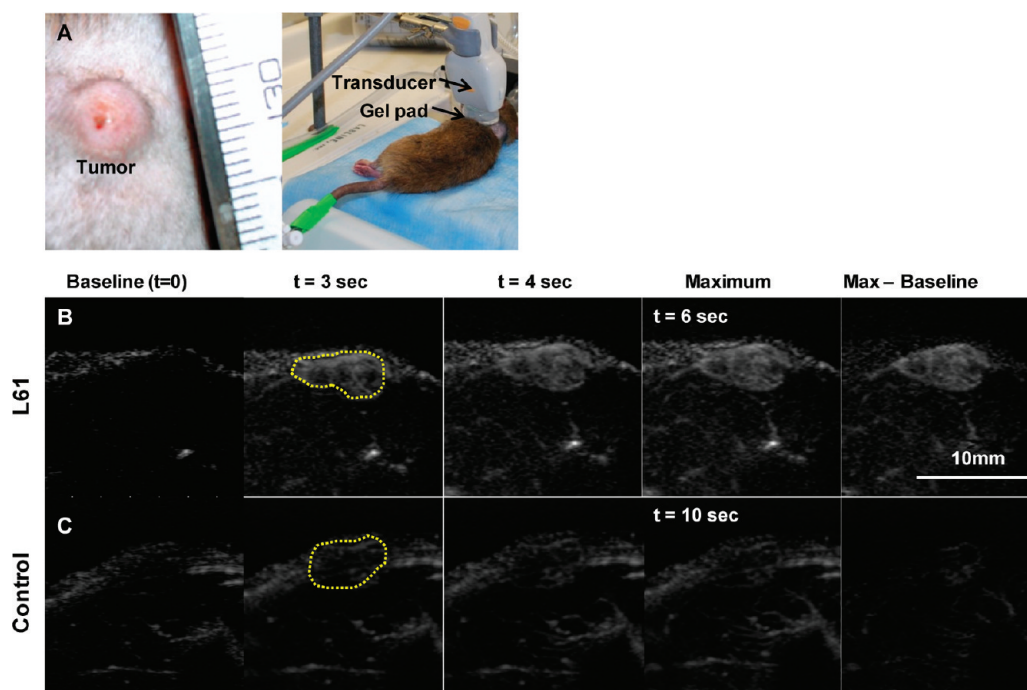
Figure 8. Tumor microflow imaging. (A) Representative subcutaneous tumor and experimental setup; (B) microflow images of tumor after L61 nanobubbles; (C) the same tumor after control microbubble administration. Dashed lines indicate the tumor location. Baseline image is the first video frame immediately after flash.
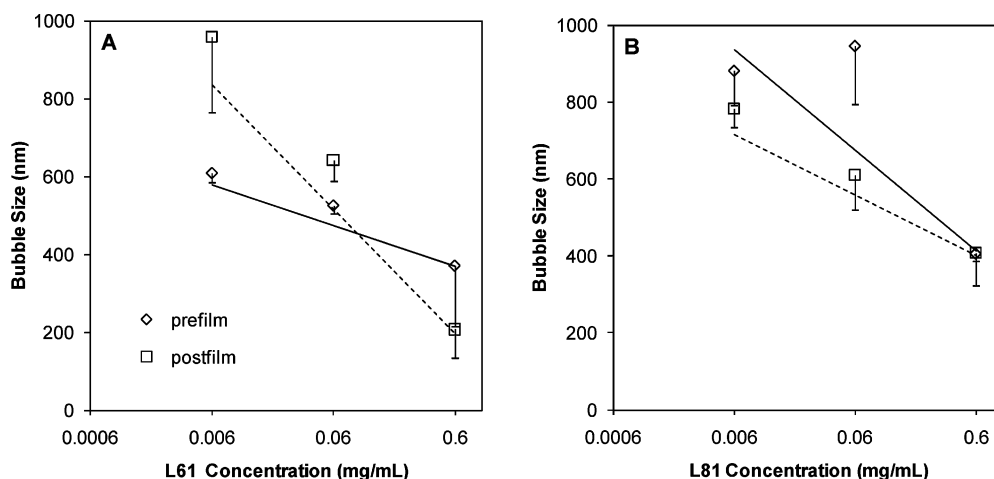

Figure 9. Bubble size dependence on Pluronic concentration. (A) L61; (B) L81.

loses its ability to control bubble size, which is in agreement with our results. In contrast, L61 and L81 are very hydrophobic and have higher membrane penetration ability, and hence are not easily squeezed out of the membrane. To accommodate that, a size decrease of the bubbles may become a necessary means for the system to stay in equilibrium.

Our results also showed that bubble size is inversely related to Pluronic concentration; this is true in all cases except Pluronic L31, which did not show any effects on bubbles size. Figure 9 demonstrates the inverse relationships between Pluronic concentration and bubble size for L81 and L61 bubbles (R^2 values of 0.96 (prefilm) and 0.86 (postfilm) for L81 and 0.93 (prefilm) and 0.88 (postfilm) for L61). While the bubble size dependence on Pluronic concentration can

be explained as above, the L31 anomaly in bubble size control in our studies can be attributed to its unique structure and size. Studies have shown that L31 has weak partitioning in unilamellar vesicle membranes.[68] This polymer, unlike the other Pluronics studied in this work, has a 16 carbon length of PO block compared to 31−41 for the other Pluronics used (Table 1). Once in the folded conformation, in order to interact with the bubble lipid shell, the shorter hydrophobic PO segment of L31 is unfavorable for packing between lipid molecules (which have primarily 17-carbon

---

(68) Santore, M. M.; et al. Effect of Surfactant on Unilamellar Polymeric Vesicles: Altered Membrane Properties and Stability in the Limit of Weak Surfactant Partitioning. *Langmuir* **2002**, *18*, 7299–7308.

hydrophobic tails). This suggests a reduced interaction of L31 with the lipid membrane.

Results also showed that the concentration of all but L31 bubbles, decreased significantly with time, suggesting that bubbles were coalescing or dissolving. The former is unlikely since these bubbles showed relative size stability with time regardless the type of Pluronic utilized. The high negative zeta potential values of these bubbles further refute the potential for coalescing with each other. The decrease in bubble concentration but relatively constant (or in the case of L61 and L81 decreasing) size distribution may be explained by the experimental technique used to obtain bubble counts, which had limited resolution and was unable to image the majority of the nanobubbles. Thus, bubble concentration change provides information on stability of relatively large bubbles. However, overall, the bubbles, particularly those made with postfilm addition of Pluronic appear to have comparable stability to that of control bubbles. While the small radius of the nanobubbles is not favorable for its stability according to the relationship $T = (\rho R^2)/(2DC_s)$ (T, microbubble persistence in the aqueous solution; ρ, gas density; R, initial radius of the bubble; D, diffusion coefficient of the gas),[69] the loss of bubble stability due to the reduction of size may be compensated by the Pluronic surfactant induced decrease in bubble surface tension, which is also a factor affecting bubble stability.[70]

While small UCA may be essential for drug and gene delivery, and contrast-enhanced imaging, the trade-off of their signal intensity has been a constant concern. Both in vitro and in vivo, ultrasound imaging studies have demonstrated that the echogenicity of our nanobubble system was not compromised compared to the control microbubbles. This may be explained by (1) a greater absolute number of nanobubbles compared to the larger control bubbles, and (2)

the Pluronic induced membrane fluidity increase which balances the loss of acoustic signal caused by bubble size reduction according to the acoustic theory.[71] Studies have shown that Pluronic is able to increase the cell membrane fluidity.[64] Although consistent trends indicating improved tumor enhancement over 20 min were seen with nanobubbles versus microbubbles, no significant differences were noted. It is possible that differences were somewhat obscured by the small tumor size and limitations of the ultrasound transducer. However, as indicated by the microflow imaging data, the nanobubbles are able to penetrate smaller venuoles and capillaries to a greater extent than their microbubble counterparts. Additional in depth examinations are needed to gather conclusive quantitative comparative data of bubble pharmacokinetics in our tumor model.

Conclusion

We have demonstrated that Pluronic triblock copolymers can be used for simple formulation of relatively stable echogenic lipid nanobubble UCA. Our results have shown that (1) Pluronic is effective in reducing bubble size, (2) the size control is dependent on Pluronic M_w, hydrophobicity and PO block length; and (3) once the appropriate Pluronic structural requirements are met, the bubble size decreased with an increase in Pluronic concentration. Furthermore, (4) the bubble stability and echogenicity do not appear to be compromised due to bubble size reduction. To the best of our knowledge, this is the first report on lipid perfluorocarbon nanobubble formulation without any manipulation of the bubbles post formation. By reducing bubble size, the applicability of lipid-shelled bubbles in molecular imaging and drug and gene delivery can be greatly enhanced.

(69) Frinking, P. J.; de Jong, N. Acoustic modeling of shell-encapsulated gas bubbles. *Ultrasound Med. Biol.* **1998**, *24* (4), 523–33.

(70) Bouakaz, A.; et al. Noninvasive measurement of the hydrostatic pressure in a fluid-filled cavity based on the disappearance time of micrometer-sized free gas bubbles. *Ultrasound Med. Biol.* **1999**, *25* (9), 1407–15.

(71) Samaddar, S. K.; De, J. N.; Sperber, D. Realistic estimate of incomplete fusion excitation function in nucleus-nucleus collisions. *Phys. Rev. C: Nucl. Phys.* **1992**, *46* (6), 2631–4.